arXiv:astro-ph/9809016v1 2 Sep 1998

RXTE Observations of the Anomalous Pulsar 4U 0142+61

Colleen A. Wilson, Stefan Dieters[1], Mark H. Finger[2], D. Matthew Scott[2], Jan van Paradijs[1]
ES 84 Space Sciences Laboratory, NASA/Marshall Space Flight Center, Huntsville, AL 35812;
colleen.wilson@msfc.nasa.gov, stefan.dieters@msfc.nasa.gov, finger@gibson.msfc.nasa.gov,
scott@gibson.msfc.nasa.gov, jvp@astro.uva.nl

ABSTRACT

We observed the anomalous X-ray pulsar 4U 0142+61 using the Proportional Counter Array (PCA) aboard the *Rossi X-ray Timing Explorer (RXTE)* in March 1996. The pulse frequency was measured as $\nu = 0.11510039(3)$ Hz with an upper limit of $|\dot{\nu}| \leq 4 \times 10^{-13}$ Hz s^{-1} upon the short term change in frequency over the 4.6 day span of the observations. A compilation of all historical measurements showed an overall spin-down trend with slope $\dot{\nu} = -3.0 \pm 0.1 \times 10^{-14}$ Hz s^{-1}. Searches for orbital modulations in pulse arrival times yielded an upper limit of $a_{\rm x} \sin i \lesssim 0.26$ lt-s (99% confidence) for the period range 70 s to 2.5 days. These limits combined with previous optical limits and evolutionary arguments suggest that 4U 0142+61 is probably not a member of a binary system.

Subject headings: pulsars: individual (4U 0142+61) — stars: neutron — x-rays: stars

1. Introduction

Most known accreting X-ray pulsars are members of high-mass X-ray binaries (HMXBs) containing an OB companion (van Paradijs 1995; Bildsten et al. 1997). Comparatively, the number of pulsars found in low-mass X-ray binaries (LMXBs) is quite small. Only five pulsars are known to be members of LMXBs: Her X–1, GX 1+4, GRO J1744–28, 4U 1626–67, and SAX J1808.4-3658 = XTE J1808-369 (Chakrabarty & Morgan 1998), which have known orbital periods or companions (Bildsten et al. 1997 and references therein.) In addition to the five known LMXB pulsars, there are 6 to 8 pulsars which are not members

[1]University of Alabama in Huntsville

[2]Universities Space Research Association

of HMXBs: 4U 0142+61, 1E 1048.1–5937, 1E 2259+586, RX J1838.4–0301 (see Mereghetti, Belloni, & Nasuti 1997 for an alternative interpretation of this system), 1E 1841–045, 1RXS J170849.0–400910 (Vasisht & Gotthelf 1997 and references therein), AX J1845–0258 (Gotthelf & Vasisht 1998), and possibly RX J0720.4–3125 (Haberl et al. 1997) . These pulsars, called anomalous or braking X-ray pulsars (van Paradijs, Taam, & van den Heuvel 1995; Mereghetti & Stella 1995; Ghosh, Angelini, & White 1997), all have spin periods in the 5-11 s range, which is extremely narrow compared to the 69 ms-2.8 hr range of spin periods of HMXB pulsars. No optical counterparts of these systems have been detected to date, and 4U 0142+61 (Steinle et al. 1987; White et al. 1987; Coe & Pightling 1998), 1E 1048.1–5937 (Mereghetti, Caraveo, & Bignami 1992), 1E 2259+586, RX J1838.4–0301 (Coe & Pightling 1998 and references therein), RX J0720.4–3125 (Haberl et al. 1997; Motch & Haberl 1998) have optical limits that rule out a high-mass companion. These pulsars are also characterized by the following properties: (1) a general spin down trend with time scales $P/|\dot{P}| = 10^3 - 10^5$ years, while HMXBs with similar periods show episodes of spin-up and spin-down (Bildsten et al. 1997); (2) No evidence of orbital periodicity to date; (3) a low X-ray luminosity of $10^{34} - 10^{36}$ ergs s^{-1} that is quite constant on time scales of days to ~ 10 years; (4) a very soft X-ray spectrum usually well described by a combination of a blackbody with effective temperature $\sim$ 0.3-0.4 keV and a photon power law ($f(E) = AE^{-\gamma}$) with photon index $\gamma = 3 - 4$ (Mereghetti, Stella, & Israel 1998); and (5) a relatively young age ($\lesssim 10^5$ yr) as inferred from the low galactic scale height (~ 100 pc r.m.s.) of the anomalous X-ray pulsars (AXPs) as a group (van Paradijs, Taam, & van den Heuvel 1995) and the apparent association of 1E 2259+587 (Fahlman & Gregory 1981), 1E 1841–045 (Vasisht & Gotthelf 1997), and RX J1838.4–0301 (Schwentker 1994) with supernova remnants.

The persistent X-ray source 4U 0142+61 was discovered with *Uhuru* (Forman et al. 1978). Pulsations at 8.7 s were discovered in 1984 August *EXOSAT* data (Israel, Mereghetti, & Stella 1994). A 25 minute modulation was also seen in these data (White et al. 1987), but was later found to be due to the nearby X-ray transient pulsar RX J1046.9+6121 (Motch et al. 1991; Hellier 1994). The *ASCA* 2-10 keV spectrum of 4U 0142+61 was well described by a blackbody with effective temperature 0.386 ± 0.005 keV plus a power law with photon index 3.67 ± 0.09 and an absorption column $N_{\rm H} = 9.5 \pm 0.4 \times 10^{21}$ cm^{-2} (White et al. 1996). This spectrum was consistent with an earlier spectrum measured with *EXOSAT* when RX J0146.9+6121 was not present (White et al. 1987). The spin frequency of 4U0142+61 was measured with *Einstein* (White et al. 1996), *EXOSAT* (Israel, Mereghetti, & Stella 1994), *ROSAT* (Motch et al. 1991; Hellier 1994), *ASCA* (White et al. 1996), and *RXTE* (this paper). The spin frequency history is shown in Figure 1. All high significance historical measurements of the spin frequency follow the general spin-down

trend of $\dot{\nu} = -3.1 \pm 0.1 \times 10^{-14}$ Hz s^{-1}, which corresponds to a spin-down timescale $\nu/|\dot{\nu}| \approx$ 123,000 yr. Three frequency measurements from 1985 EXOSAT post discovery data and 1991 ROSAT data (Israel, Mereghetti, & Stella 1994), which Israel et al. (1994) found to have high probabilities of chance occurrence, have been omitted from Figure 1.

Israel et al. (1994) performed an orbital period search on $\sim$ 12 hr of *EXOSAT* ME data from 1984 August 27-28. The search was carried out for periods from 430 s to 43,000 s, assuming a circular orbit. No significant orbital signature was found. Other *EXOSAT* measurements in 1985 November and December did not have sufficient time resolution to unambiguously detect 4U 0142+61.

Here we present results from *RXTE* observations of 4U 0142+61, obtained in 1996 March. The observation times and durations are listed in Table 1. An orbital period search is performed for periods between $\sim$ 600 s and 4.6 days. Power spectra are presented and compared to white noise spectra with identical windowing. Upper limits are placed on the size of the allowed orbits for different trial periods. Next a modified algorithm is used to search for orbital periods shorter than $\sim$ 600 s and to place upper limits on the size of allowed orbits. *RXTE* results are compared to previous results obtained with *EXOSAT*. Allowed companion types based upon these orbital limits and previous optical limits are discussed.

2. Observations and Analyses

The Proportional Counter Array (PCA) on *RXTE* consists of five xenon/methane multi-anode proportional counters sensitive to photons from 2-60 keV and has a total collecting area of 6500 cm^2. The PCA is a collimated instrument with an approximately circular field-of-view with a FWHM of about 1° (Jahoda et al. 1996). PCA observations of 4U 0142+61 were performed on 1996 March 25 and 28-30. Details of these observations are given in Table 1. The field of view also contained the Be/X-ray pulsar RX J0146.9+6121 (Motch et al. 1991; Hellier 1994; Haberl et al. 1998). For 1996 March 28-30, Good Xenon data (time and detector tagged events with 1 μs time resolution and full energy resolution) were used for our analysis. For 1996 March 25, Event Mode data, which have lower time resolution and similar energy resolution, were used. To maximize signal to noise ratio, data from only the top xenon layer of the PCA and from the energy range 3.7-9.2 keV were selected. The light curves were binned to 125 ms time resolution and the times were corrected to the solar system barycenter.

The pulse frequency of 4U 0142+61 was determined to be $\nu_{\rm spin} = 0.11510051(8)$ by an

epoch-folded search of data from 1996 March 25 and 28-30 for the frequency range 0.1139 - 0.1165 Hz. Assuming the pulse frequency remained constant at this value across our observations, we divided the data into segments and determined phase offsets and intensities for each segment. A template profile was created by epoch-folding the first 80,000 seconds of data from March 28-30. The template profile is shown in Figure 2. The data were then divided into 250 second segments. In each segment the data were epoch-folded at the pulse frequency. The template and the pulse profiles from each segment were represented by a Fourier expansion in pulse phase. The profiles were limited to the first 3 Fourier coefficients, which contained 98.6% of the power in the template. These Fourier coefficients, a_k, were calculated as

$$a_k = \frac{1}{N} \sum_{j=1}^{N} R_j e^{-i2\pi jk/N} \tag{1}$$

where k is the harmonic number, $i = (-1)^{1/2}$, $N = 16$ is the number of phase bins in the pulse profile, and R_j is the count rate in the jth bin of the pulse profile. The pulse phase offset of each segment with respect to the template was calculated by cross-correlating each phase fold with the template. The cross-correlation is equivalent to a fit to

$$\chi^2 = \sum_{k=1}^{3} \frac{|a_k - Ie^{i2\pi k\phi} t_k|^2}{\sigma_{a_k}^2} \tag{2}$$

where t_k is the Fourier coefficient of harmonic number k of the template profile, I is the relative intensity of the measured profile with respect to the template, and ϕ is the phase offset of the measured profile relative to the template profile. The errors on the phase offsets were weighted according to the amount of data in each segment. Figure 3 shows the phase offsets with a best fit quadratic removed. A total of 7 points, which deviated from this fit by more than 0.25 cycles, were discarded. For 5 of these outliers, the 250 s bins were less than 1/3 full. The remaining two outliers, which both contained less than 200 s of data and were offset by about 1/2 cycle, contained double-peaked pulse profiles. A quadratic fit to the remaining points yielded a best fit frequency of $\nu = 0.11510039(3)$ Hz at MJD 50169.835 (consistent with our earlier epoch-folding results) and a 3 σ upper limit of $\dot{\nu} \lesssim 4 \times 10^{-13}$ Hz s^{-1} with $\chi^2/182 = 1.05$.

The phase offsets were searched for an orbital periodicity using a Lomb-Scargle periodogram (Press et al. 1992 and references therein) shown in Figure 4. The top panel is the Lomb-Scargle periodogram for the entire 4 day interval. The largest peak at ≈ 586 s has a probability of chance coincidence of 65%. The center panel is the Lomb-Scargle periodogram for March 28-30 only. The largest peak at ≈ 1680 s has a probability of chance coincidence of 78%. These probabilities were computed using Monte-Carlo simulations of 10,000 white noise realizations. The phase offsets were simulated as white noise with zero

mean and standard deviations equal to the measurement errors on the phase offsets along with the actual time tags corresponding to the phase offsets. The cumulative probability distribution of the peak noise power was generated by retaining the power in the largest noise peak for each trial. The bottom panel is the Lomb-Scargle periodogram for white noise with mean and variance equal to that of the phase offsets with time tags corresponding to the 4 day interval. From the noise power, it is evident that much of the higher frequency variability in the power spectra is due to the windowing of the data. The Lomb-Scargle technique removes a constant from the data. Any variations in count rate that deviate from a constant result in low frequency variations in the power spectrum. This analysis revealed no significant orbital signatures.

Previous upper limits, $a_{\rm x} \sin i \lessapprox 0.37$ lt-s (430 s $\lessapprox P_{\rm orb} \lessapprox$ 43000 s) estimated from *EXOSAT* data by Israel et al. (1994), were calculated using the method of Van der Klis (1989) . This method assumes that the total power in a frequency bin is the sum of the signal power and the noise power. Vaughan et al. (1994) show that this assumption holds if a large number, n, of power spectra have been averaged together. However, if n is small or $n = 1$, as is the case for *EXOSAT* and *RXTE* measurements of 4U 0142+61, this assumption is incorrect. For small values of n, the total power is calculated from the vector sum of the Fourier amplitudes of the signal and noise. Vaughan et al. (1994) estimate that upper limits calculated using van der Klis (1989) will increase by at least 30% when calculated correctly.

Upper limits for $a_{\rm x} \sin i$, the projected semi-major axis of the neutron star, were calculated under the assumption that signal and noise amplitudes are combined vectorially. No intrinsic spin frequency variations were detected, hence the pulse phase was given by

$$\phi = \phi_0 + \nu_0 t^{\rm em} \tag{3}$$

were ϕ_0 is a constant phase and ν_0 is a constant frequency. The pulse emission time $t^{\rm em} = t^{\rm ssb} - z$ where $t^{\rm ssb}$ is the time corrected to the solar system barycenter and z is the time delay due to binary motion. For a circular orbit the delay is given by,

$$z = a_{\rm x} \sin i \cos\left(\frac{2\pi(t^{\rm em} - T_{\pi/2})}{P_{\rm orb}}\right) \tag{4}$$

where $P_{\rm orb}$ is the orbital period and $T_{\pi/2}$ is the epoch of 90° mean orbital longitude.

The phase offsets were modeled for an arbitrary epoch t_0 (chosen as the mid-time of the data set) as

$$\phi_{\rm model} = \phi_0 + \Delta\nu_0(t - t_0) + A\cos\left(\frac{2\pi(t - t_0)}{P_{\rm orb}}\right) + B\sin\left(\frac{2\pi(t - t_0)}{P_{\rm orb}}\right) \tag{5}$$

for a fixed value of the trial orbital period $P_{\rm orb}$, where ϕ_0 was a constant offset in phase and $\Delta\nu_0$ is an offset in frequency. In this model,

$$a_{\rm x} \sin i = \frac{(A^2 + B^2)^{1/2}}{\nu_0 \,{\rm sinc}\,(\frac{\pi \Delta T}{P_{\rm orb}})} \tag{6}$$

where ν_0 is the frequency used for epoch folding, ${\rm sinc}\; x = \frac{\sin x}{x}$ and $\Delta T = 250$ s, the bin size. The loss of sensitivity for short periods is accounted for by the ${\rm sinc}\,(\pi \Delta T / P_{\rm orb})$ windowing factor. The phase and frequency offsets, ϕ_0 and $\Delta\nu_0$, were estimated for each orbital period, accounting for the loss of sensitivity at long orbital periods. For each trial orbital period, single parameter 99% confidence regions were constructed for A and B (Lampton, Margon, & Bowyer 1976). Since $A = B = 0$ was not excluded for any trial orbital periods, an upper limit for $a_{\rm x} \sin i$ was estimated from the maximum value of $(A^2 + B^2)^{1/2}$, the point on the confidence region farthest from the origin. Upper limits on $a_{\rm x} \sin i$ at 99% confidence generated in this manner are shown in Figure 5. Sensitivity is reduced for periods $\lesssim 600$ seconds, for periods $\gtrsim 10^5$ seconds, and at the *RXTE* orbital period (≈ 96 min). An overall 99% upper limit for a selected frequency range can be estimated from the largest upper limit within that range. For all periods in the range 587 s $\lesssim P_{\rm orb} \lesssim 2.5$ days, $a_{\rm x} \sin i \lesssim 0.27$ lt-s (99% confidence). If we exclude the region of reduced sensitivity around the *RXTE* orbital period, this limit reduces to 0.25 lt-s (99% confidence).

To search for orbital periods shorter than about 600 seconds, a different method was employed. Well defined phase offsets and intensities could not be computed by cross-correlating profiles and the template for segments much shorter than 250 seconds. However, if the intensity was assumed to be known, phase offsets could be computed for much shorter intervals by approximating the cross-correlation function with a linear model. The intensity of 4U 0142+61 appeared to be reasonably constant on short time scales, so we assumed it was constant across 500 s intervals. Intervals 500 s long produced very good measurements of the phase offset and intensity, while allowing longer timescale intensity variations. Phase offsets and relative intensities were generated for each 500 second interval by the cross-correlation method described earlier. Next each 500 s interval was subdivided into shorter segments, each 2 pulse periods long (≈ 17.4 seconds). Fourier coefficients were then fit to each 17.4 s segment by minimizing

$$\chi^2 = \sum_{i=1}^{N} \frac{\{r_i - [c_0 + \sum_{k=1}^{3} u_k \cos(2\pi k \phi(t)) + v_k \sin(2\pi k \phi(t))]\}^2}{\sigma_{r_i}^2} \tag{7}$$

where r_i is count rate measurement i, N is the number of measurements in a 17.4 s segment, c_0 is a constant offset, k is the harmonic number, u_k and v_k are the Fourier coefficients, and $\phi(t) = \phi_0 + \nu_0 (t - t_0)$ is the phase model. The Fourier coefficients then were fit by a

linearized model of the cross-correlation with χ^2 given by

$$\chi^2 = \sum_{k=1}^{3} \frac{|a_k - I_{500}(1 + 2\pi i k \Delta\phi) t_k|^2}{|\sigma_{a_k}|^2} \tag{8}$$

where $a_k = u_k - iv_k$, t_k is the template, I_{500} is the intensity for the corresponding 500 s interval, and $\Delta\phi$ is the phase offset for each 17.4 s segment. The mean of the phase offsets for all 17.4 s segments within a 500 s interval corresponded to the phase offset computed for that 500 s interval using the cross-correlation method. The top panel of Figure 6 shows the Lomb-Scargle periodogram generated from the short interval phases. The largest peak at $\approx$ 87 s has a probability of chance coincidence of 18%. The bottom panel of Figure 6 shows the 99% confidence upper limits on $a_{\rm x} \sin i$ for fixed trial orbital periods. For the period range, 70 s $\lesssim P_{\rm orb} \lesssim$ 610 s, $a_{\rm x} \sin i \lesssim 0.26$ lt-s at 99% confidence.

EXOSAT ME data with 1 second time resolution from 1984 August were obtained from the High Energy Astrophysics Science Archive Research Center (HEASARC). Spacecraft position information was not easily obtainable, so the times were corrected only for motion of the Earth. The data in 1000 second segments were epoch-folded at the period $P_{\rm spin} = 8.68723(4)$ s measured by Israel et al. (1994). A template profile was generated by epoch-folding the entire data set at the pulse period. The template and the pulse profiles from each segment were represented by a Fourier expansion in pulse phase. The pulse phase offset of each segment with respect to the template was calculated by cross-correlating each phase fold with the template. The phase offsets then were searched for an orbital periodicity using a Lomb-Scargle periodogram. No significant orbital signatures were found. Using the method described earlier, upper limits were placed on $a_{\rm x} \sin i$. For all periods in the range 2050 s $\lesssim P_{\rm orb} \lesssim$ 2 days, $a_{\rm x} \sin i \lesssim 0.73$ lt-s (99% confidence). This limit, generated under the assumption that signal and noise amplitudes are combined vectorially, is about twice the limit of $a_{\rm x} \sin i \lesssim 0.37$ lt-s (99% confidence) obtained by Israel et al. (1994) . The latter was obtained under the assumption (van der Klis 1989) that signal power and noise power may be added, which does not apply in this case.

3. Discussion

The limits on $a_{\rm x} \sin i$, in conjunction with an assumed inclination angle and an assumed neutron star mass of 1.4 $M_\odot$, can be recast to give a limit at each orbital period on the companion mass. These limits include no assumptions as to the nature of the companion. A plot of these limits, for inclination angles of 8, 30, and 90° versus orbital period is shown in Figure 7.

In a low-mass X-ray binary, the companion is expected to fill its Roche Lobe. Eggleton (1983) gave a useful expression for the Roche Lobe radius, given by

$$\frac{R_2}{a} = \frac{0.49q^{2/3}}{0.6q^{2/3} + \ln(1+q^{1/3})} \tag{9}$$

where a is the separation between the two stars, $q = M_2/M_{\rm x}$ is the mass ratio, M_2 is the companion mass, and $M_{\rm x}$ is the neutron star mass. This expression can be combined with Kepler's third law to obtain the binary period as a function of the companion star's average density, $\bar{\rho} = 3M_2/4\pi R_2^3$ and mass ratio q, given by

$$P_{\rm binary} = 3 \times 10^4 \,{\rm s} \left(\frac{\bar{\rho}}{\bar{\rho}_\odot}\right)^{-1/2} \left(\frac{q}{1+q}\right)^{1/2} (0.6 + q^{-2/3}\ln(1+q^{1/3}))^{3/2} \tag{10}$$

where $P_{\rm binary}$ is the binary period. If the structure of the Roche Lobe filling star is assumed, and thus a relation between its mass and radius, the binary period can be expressed as a unique function of the mass, M_2, for an assumed value of $M_{\rm x} = 1.4M_\odot$. Period-mass relations derived assuming a normal main sequence star, a helium main sequence star, a white dwarf (Verbunt & van den Heuvel 1995) and a period core mass relation for low mass ($\lesssim 2M_\odot$) giants (Phinney & Kulkarni 1994) are listed in Table 2 and plotted in Figure 7. The period core mass relation for low mass giants is valid for core masses of $0.16M_\odot \lesssim M_{\rm core} \lesssim 0.45M_\odot$, where the lower limit corresponds to the helium core mass at the end of main sequence evolution and the upper limit is the core mass at helium flash (Phinney & Kulkarni 1994).

The maximum allowed mass of a Roche lobe filling hydrogen main sequence companion is $\sim 0.25M_\odot$ for inclinations greater than 30° (99% confidence). This mass corresponds to an M5 or later type star. Larger masses are allowed if the inclination angle is quite small. For $i = 8°$ the maximum mass is $\sim 0.5M_\odot$ (99% confidence). The probability of observing a system with $i < 8°$ by chance is 1%. If instead, a Roche lobe filling helium burning companion is assumed, higher masses (99% confidence) of $\sim 0.65M_\odot$ for $i > 30°$ and $2M_\odot$ for $i = 8°$ are allowed. Low mass giants, similar to the companion to GRO J1744-28 (Finger et al. 1996), with core masses of $\sim 0.21M_\odot - 0.45M_\odot$ are allowed for $i > 30°$ and core masses of $\sim 0.18M_\odot - 0.45M_\odot$ are allowed for $i > 8°$. Period-mass relations predict white dwarf masses well below our upper limits for all inclinations.

Optical (V $\gtrsim$ 24, Steinle et al. 1987; R $\gtrsim$ 22.5, White et al. 1987) and infra-red (J $\gtrsim$ 19.6 and K $\gtrsim$ 16.88, Coe & Pightling 1998) observations failed to detect any counterpart within the *ROSAT* error circle (Hellier 1994). The optical limits can be used to further constrain the allowed companion masses based upon calculated optical magnitudes of a normal main sequence star, helium main sequence star, and the optical emission produced

by reprocessed X-rays in the accretion disc. The column density, $N_H = 8 \times 10^{21}$ cm^{-2} measured by White et al. (1996) , corresponds to an optical extinction of $A_v \sim 4.7$ (Predehl & Schmitt 1995), which implies a distance of ~ 5 kpc (Hakkila et al. 1997). However, the dust scattering halo observed by *ROSAT* (White et al. 1996) was only half that predicted by N_H, suggesting that the absorbing material is clumped along the line of sight and that 4U 0142+61 is most likely at a distance of < 5 kpc. A main sequence companion with a mass of $\lesssim 0.8 M_\odot$ (for any inclination angle) is compatible with the optical limits.

The optical observations place much more stringent constraints on a giant companion with a helium core and on a helium main sequence companion. The minimum core mass for a giant star with a helium core is $0.16 M_\odot$, corresponding to the core mass when the star leaves main sequence. A giant of solar metalicity with a core mass of 0.16 $M_\odot$ has a luminosity of $L \simeq L_\odot$ and an effective temperature of $\sim$ 5000 K (Phinney & Kulkarni 1994). At the upper limit distance of 5 kpc with absorption $A_v \sim 4.7$ and a bolometric correction of -0.2 (Zombeck 1990), we calculate an apparent magnitude of $V \sim 23$, for a giant star with a core mass of $0.16 M_\odot$. Hence a giant companion similar to that of GRO J1744-28 is not allowed by the optical limits. The minimum mass for a helium main sequence star is $M \sim 0.3 M_\odot$ (Kippenhahn & Weigert 1990). From plots in Kippenhahn & Weigert (1990), a $0.4 M_\odot$ He star corresponds to a luminosity of $\sim 5.6 L_\odot$ and an effective temperature of $\sim$ 30,000 K. At the upper limit distance of 5 kpc with absorption $A_v \sim 4.7$ and bolometric correction of -3 (Flower 1996), we calculate an apparent magnitude $V \sim 24$ for a $0.4 M_\odot$ helium star. Hence a helium star of a mass of $\lesssim 0.4 M_\odot$ is compatible with optical limits.

In low-mass X-ray binaries, the optical emission is usually dominated by reprocessing of X-rays in the accretion disk. From fits to several low-mass X-ray binaries with known distances, van Paradijs and McClintock (1994) derived an empirical relationship between the absolute visual magnitude and the X-ray luminosity and orbital period. This relationship assumes that the companion is filling its Roche-lobe, the optical emission is dominated by the accretion disk, and that accretion disks are axially symmetric scaled up versions of a standard shaped toy model. No assumptions are made about the companion type. This relationship is given by

$$M_{\rm v} = 1.57 - 2.27 \log \left[\left(\frac{P}{1{\rm hr}} \right)^{2/3} \left(\frac{L_{\rm x}}{L_{\rm Edd}} \right)^{1/2} \right] \tag{11}$$

where $M_{\rm v}$ is the absolute visual luminosity, P is the binary period, $L_{\rm x}$ is the X-ray luminosity, and $L_{\rm Edd} = 2.5 \times 10^{38}$ erg s^{-1} is the Eddington luminosity. Using this relation along with estimates of the X-ray luminosity, $L_{\rm x} = 7.2 \times 10^{34}$ d$^2_{\rm kpc}$ (White et al. 1996), absorption $A_{\rm v} \sim 4.7$ (White et al. 1996), and apparent visual magnitude $V \gtrsim 24$ (Steinle et

al. 1987), we derived a relation between binary period P, and distance d. If the disk was fainter than the observed optical limit, then the allowed orbital periods are given by

$$P \lesssim 12.5\eta \text{ s } \left(\frac{d}{1\text{kpc}}\right)^{1.81} \tag{12}$$

where η is an estimate of the scatter in the van Paradijs & McClintock relationship. From Figure 2 in Van Paradijs & McClintock (1994), we estimate a scatter in M_v of ~ 0.75 magnitudes in the data used to obtain equation (11). A decrease in M_v of 1.5 magnitudes (twice the scatter), results in an increase in the maximum period by a factor of $\eta \simeq 10$. Thus, for the upper limit distance of 5 kpc (where $L_{\rm x} = 2 \times 10^{36}$ erg s^{-1}, at which equation (11) applies) this relation, including scatter, requires a period $P \lesssim 2300$ s. Substituting this into the period-mass relationships in Table 2, results in allowable masses for only helium main sequence companions and white dwarf companions at 5 kpc. At distances $\lesssim 3$ kpc, which are more likely based upon *ROSAT* scattering measurements (White et al. 1996), only white dwarf companions are allowed.

4. Conclusion

We found no evidence (99% confidence) for orbital modulation in the pulse arrival times for orbital periods between 70 seconds and 2.5 days. Searches for orbital modulations in pulse arrival times yielded an upper limit of $a_{\rm x} \sin i \lesssim 0.26$ lt-s (99% confidence) for the period range 70 s to 2.5 days. Our limits on $a_{\rm x} \sin i$ lead to 99% confidence dynamical limits for $i \gtrsim 30^\circ$ of $\lesssim 0.25 M_\odot$ for normal main sequence companions, $\lesssim 0.65 M_\odot$ (99% confidence) for helium main sequence companions, and $0.21 M_\odot \lesssim M_{\rm core} \lesssim 0.45 M_\odot$ (99% confidence) for $\lesssim 2 M_\odot$ giants with helium cores. Optical limits at 5 kpc allow masses of $\lesssim 0.8 M_\odot$ and $\lesssim 0.4 M_\odot$ for normal and helium main sequence companions respectively. Optical limits do not allow giant companions with helium cores. Optical and dynamical limits currently do not constrain white dwarf companions.

The smooth spin-down (Figure 1) observed in 4U 0142+61 is inconsistent with the random walk behavior expected for wind fed accreting pulsar (Bildsten et al. 1997). Hence, 4U 0142+61 is unlikely to be a wind accretor. Long-term observations with BATSE (Bildsten et al. 1997) show that disk fed accreting pulsars switch between states of spin-up and spin-down with the magnitude of the torque in either state comparable to a characteristic torque. A pulsar subject to this torque will spin up (or down) at a rate of (Bildsten et al. 1997)

$$|\dot{\nu}| \lesssim 1.6 \times 10^{-13} \text{ Hzs}^{-1} \left(\frac{\dot{M}}{10^{-10} M_\odot \text{ yr}^{-1}}\right) P_{\rm spin}^{1/3} \tag{13}$$

where $\dot{M}$ is the mass accretion rate and $P_{\rm spin}$ is the pulsar spin period in seconds. The observed spin-down rate of $\dot{\nu} = -3 \times 10^{-14}$ Hz s^{-1} corresponds to $\dot{M} \gtrsim 9 \times 10^{-12} M_{\odot}$ yr^{-1} or a luminosity of $L \gtrsim 10^{35}$ erg s^{-1} which is consistent with the luminosity of $7.2 d_{\rm kpc}^2 \times 10^{34}$ erg s $^{-1}$ measured with *ASCA* (White et al. 1996). Hence the observed long-term spin-down rate of 4U 0142+61 is consistent in behavior with the disk fed accreting pulsars. However, optical limits only allow accretion disks in systems with orbital periods $\lesssim 2300$ s. Orbital periods this small allow only helium main sequence and white dwarf companions at distances of 3-5 kpcs and only white dwarf companions at $\lesssim 3$ kpc,which are more likely based upon *ROSAT* scattering measurements (White et al. 1996). However, current evolutionary scenarios do not provide a mechanism for producing a Roche lobe filling white dwarf companion or a Roche lobe filling helium main sequence companion within the assumed $\lesssim 10^5$ yr age of the system. This age is based upon the low scale height of AXPs as a group (van Paradijs, Taam, & van den Heuvel 1995) and ages inferred from supernova remnant associations of other AXPs.

Optical, dynamical, and evolutionary limits argue against binarity in AXPs. Van Paradijs et al. (1995) proposed that AXPs are powered by accretion onto the neutron star from a circumstellar disc resulting from a common envelope evolution. It is not clear, however, why such an evolution would result in such a narrow range of pulse periods. The narrow period range is much more easily explained by the magnetar model (Thomson & Duncan 1996). In this model, the neutron star surface is heated by the decay of the very strong magnetic field, producing X-rays. Heyl & Hernquist (1997) also propose a model consisting of a highly magnetized young neutron star surrounded by a thin envelope of hydrogen or helium. In this model, X-rays are produced by thermal emission. Pulsations are produced by a temperature gradient on the neutron star's surface induced by the strong magnetic field combined with limb darkening in the neutron star's atmosphere. Detailed long-term monitoring observations of the AXPs are needed to search for spin-up episodes which would suggest the system is an accretor, or a glitch accompanied by a soft-gamma repeater burst (Thomson & Duncan 1996), which would suggest the magnetar model.

This research made use of data obtained from the High Energy Astrophysics Science Archive Research Center (HEASARC) at the NASA Goddard Space Flight Center. JVP acknowledges support from NASA grants NAG5-3672 and NAG5-7105.

REFERENCES

Bildsten, L. et al. 1997, 113, 367

Chakrabarty, D. & Morgan, E. H. 1998, IAU Circ., No. 6877

Coe M.J., & Pightling S.L., 1998, MNRAS, in press, preprint astro-ph/9804334

Eggleton, P. P 1983, ApJ, 268, 368

Fahlman, G. G. & Gregory, P. C. 1981, Nat 293, 202

Finger, M. H. et al. 1996, Nat, 381, 291

Flower, P. J. 1996, ApJ, 469, 335

Forman, W. et al. 1978, ApJS, 38, 357

Gotthelf, E. V. & Vasisht, G. 1998, New Astronomy, 3, 293

Ghosh, P., Angelini, L., & White, N. E. 1997, ApJ, 478, 713

Haberl, F., Motch, C., Buckley, D. A. H., Zickgraf, F. -J., & Pietsch, W. 1997, A&A, 326, 662

Haberl, F., Angelini, L., Motch, C., & White, N. E. 1998, A&A, 330, 189

Hakkila, J., Myers, J. M., Stidham, B. J., & Hartmann, D. H. 1997, AJ, 114 (5),2043

Heyl, J. S. & Hernquist, L. 1997, ApJ, 489, L67

Hellier, C. 1994, MNRAS 271, L21

Israel, G. L., Mereghetti, S., & Stella, L. 1994, ApJ, 433, L25

Jahoda, K., Swank, J. H., Giles, A. B., Stark, M. J., Strohmayer, T. E., Zhang, W. & Morgan, E. H. 1996, in SPIE 2808, EUV, X-ray and Gamma-ray Instrumentation for Space Astronomy VII, ed. O. H. W. Siegmund & M. A. Grummin, (SPIE: Bellingham), 59

Kippenhahn, R. & Weigert, A. 1990, Stellar Structure and Evolution, (Springer-Verlag: New York), 216

Lampton, M., Margon, B., & Bowyer, S. 1976, ApJ, 208, 177

Mereghetti, S., Belloni, T., Nasuti, F. P. 1997 A&A,321, 835

Mereghetti, S., Caraveo, P., & Bignami, G. F. 1992, A&A, 263, 172

Mereghetti S., Stella L.,& Israel G.L. 1998,The Active X-ray Sky: Results from BeppoSAX and Rossi-XTE, Nuclear Physics B Proceedings Supplements, eds. L. Scarsi, H. Bradt, P. Giommi, & F. Fiore, Elsevier Science, in press, (preprint astro-ph/9712254)

Mereghetti, S. & Stella, L. 1995, ApJ, 442, L17

Motch, C. et al. 1991, A&A 246, L24

Motch, C. & Harberl, F. 1998, A&A, 333, L59

Phinney, E. S. & Kulkarni, S. R. 1994, Annu. Rev. Astron. Astrophys., 32, 591

Predehl, P. & Schmitt, J. H. 1995, A&A, 293, 889

Press, W. H. et al. 1992, in Numerical Recipes in Fortran, Second Edition, (Cambridge University Press: New York), 569

Rappaport S., Nelson L.A., Ma C.P., & Joss P.C., 1987, ApJ 322, 842.

Schwentker, O. 1994, A&A, 286, L47

Shu, F. H. 1982, The Physical Universe, (University Science Books: Mill Valley, CA), 150

Steinle, H., Pietsch, W., Gottwald, M., & Graser, U. 1987, Ap&SS, 131, 687

Thompson, C. & Duncan, R. C. 1996, ApJ, 473, 322

van Paradijs, J. 1995 in X-Ray Binaries, eds. W. H. G. Lewin, J. van Paradijs, & E. P. J. van den Heuvel, (Cambridge University Press: New York), 536

van Paradijs, J. & McClintock, J. E. 1994, ApJ, 463, L83

van Paradijs, J., Taam, R. E., & van den Heuvel, E. P. J. 1995, A&A 299, L41

van der Klis, M. 1989, in Timing Neutron Stars, ed. H. Ogleman & E. P. J. van den Heuvel (Dordrect: Kluwer), 27

Vasisht, G. & Gothelf, E. V. 1997, ApJ, 486, L129

Vaughan, B. A. et al. 1994, ApJ, 435, 362

Verbunt, F., & van den Heuvel, E.P.J., 1995, in *X-Ray Binaries* eds. W.H.G. Lewin, J. van Paradijs, & E.P.J van den Heuvel, (Cambridge Univ. Press: New York), 457.

White, N. E. et al. 1987, MNRAS 226, 645

White, N. E. et al. 1996, ApJ 463, L83

Zombeck, M. V. 1990, Handbook of Space Astronomy & Astrophysics, Second Edition, (Cambridge Univ. Press: New York), 70

This preprint was prepared with the AAS LaTeX macros v4.0.

Table 1: 1996 *RXTE* Observations of 4U 0142+61

Observation Start (TT)	Observation Stop (TT)	Observation Duration (ksec)
March 25:12:31:04	14:14:06	5.533
March 28:22:15:12	March 29:00:02:06	3.367
March 29:00:11:28	06:46:06	13.987
March 29:07:23:28	11:34:06	10.182
March 29:22:18:40	March 30:03:34:06	11.104

Table 2: Derived Mass-Orbital Period Relations for LMXBs[a]

Companion Type	Mass-Orbital Period Relation
Giant with He core[b]	$P_{\rm orb} = 1.1 \times 10^5$ s $(M_{\rm core}/0.16 M_\odot) f(q)$[c]
H Main Sequence	$P_{\rm orb} = 3 \times 10^4$ s $(M_{\rm c}/M_\odot) f(q)$
He Main Sequence	$P_{\rm orb} = 3 \times 10^3$ s $(M_{\rm c}/M_\odot) f(q)$
White Dwarf	$P_{\rm orb} = 40$ s $(M_\odot/M_{\rm c})$[d]

[a] Adapated from Verbunt and van den Heuvel (1995)

[b] Valid for $0.16 M_\odot \lesssim M_{\rm core} \lesssim 0.45 M_\odot$ (Phinney & Kulkarni 1994)

[c] $f(q) = (1 + 1/q)^{-1/2} (0.6 + q^{-2/3} \ln(1 + q^{1/3}))^{3/2}$

[d] For $q < 0.8$, (i.e. $M_c < 1.1 M_\odot$), $f(q) \approx 1$

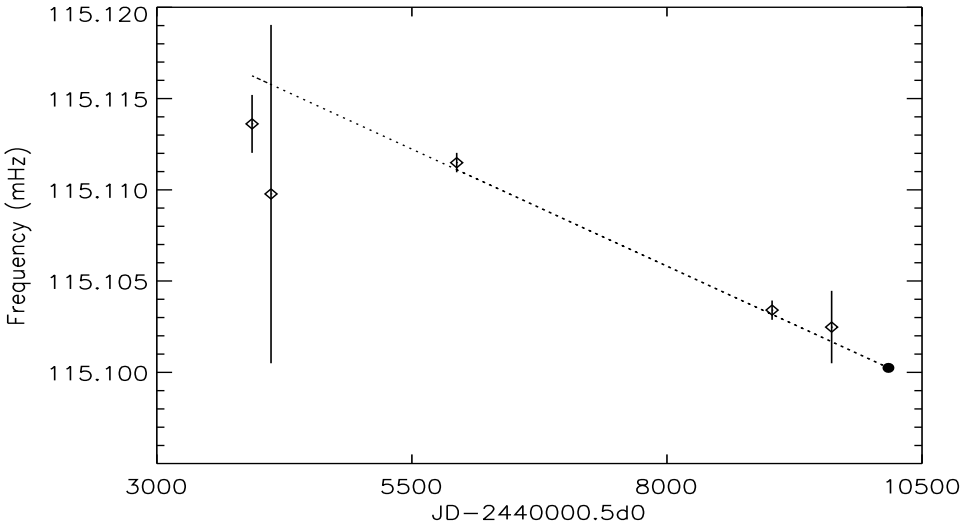

Fig. 1.— The historical pulse frequency history. The *RXTE* measurement is indicated by a filled circle. The dotted line is the best linear fit to the overall spin down $\dot{\nu} = -3.1 \pm 0.1 \times 10^{-14}$ Hz s^{-1}.

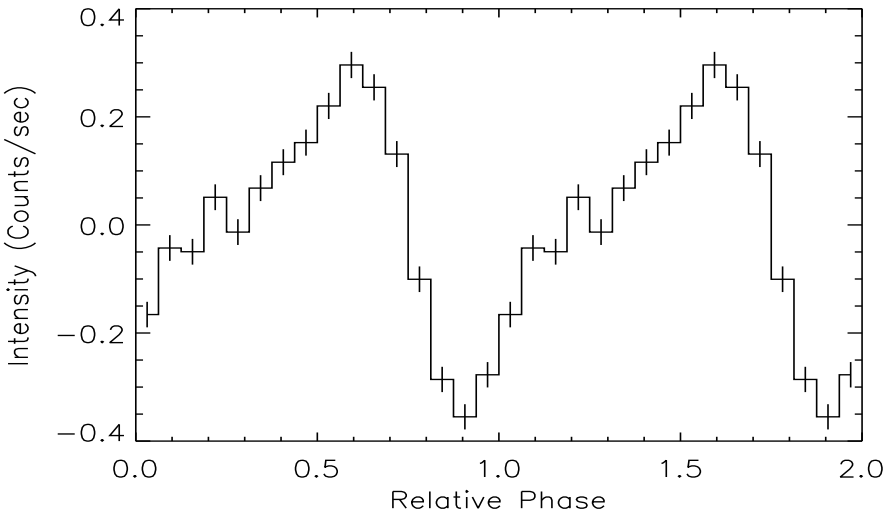

Fig. 2.— The mean-subtracted template pulse profile generated by epoch-folding the first 80,000 s of 3.7-9.2 keV data from March 28-30 at a constant frequency, $\nu_{\rm spin}$=0.11510041 Hz.

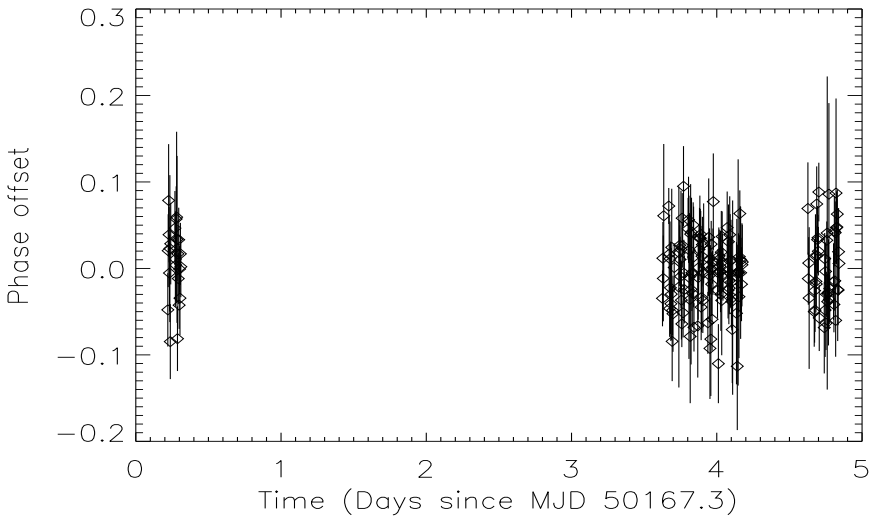

Fig. 3.— Phase offsets for 250 s intervals of data from 1996 March 25-30. A best fit quadratic has been subtracted. The time plotted is in days since 1996 March 25:07:12:00 (MJD 50167.3).

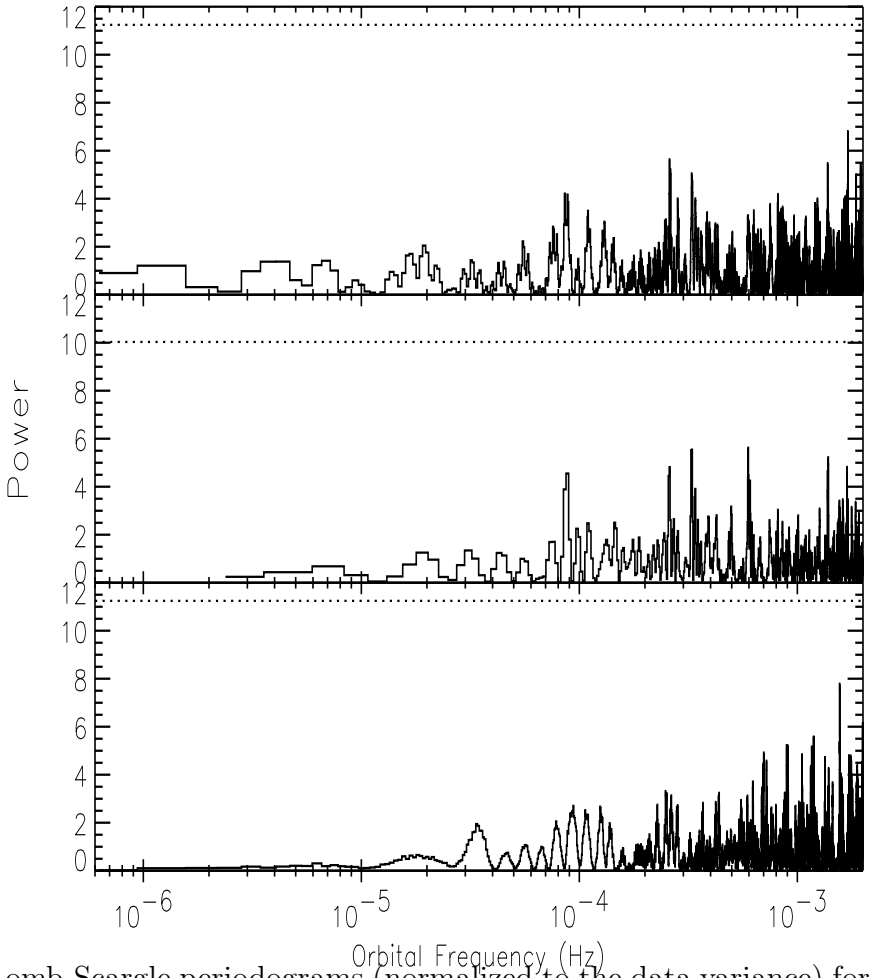

Fig. 4.— Lomb-Scargle periodograms (normalized to the data variance) for the entire March 25-30 data set (top panel), the March 28-30 dataset only (center panel), and white noise (bottom panel) with mean and variance equal to that of the phase offsets and time tags corresponding to the March 25-30 interval. The dotted lines indicate the 99% confidence level for a detection.

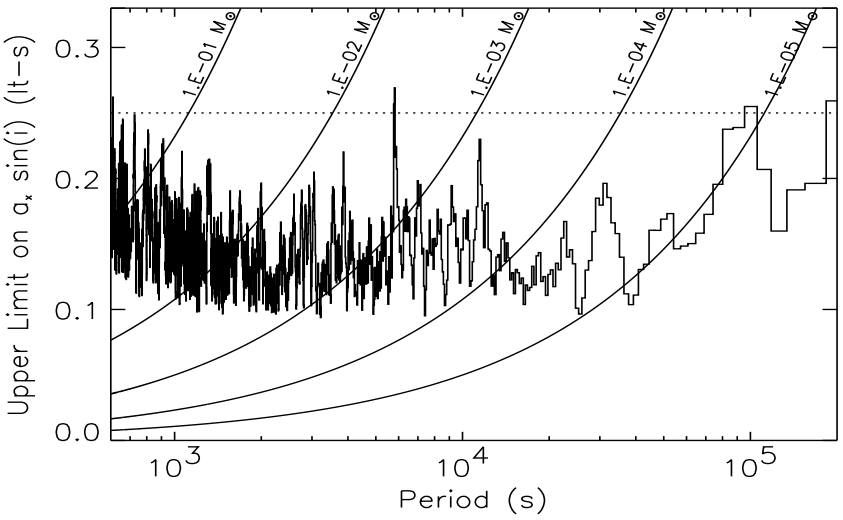

Fig. 5.— Upper limits to $a_{\rm x} \sin i$ (99% confidence) for a circular orbit at a trial orbital period. Sensitivity is reduced for both the longest and shortest trial orbital periods. Removal of data containing Earth occultations also reduces sensitivity at the *RXTE* orbital period. Curves of constant mass function are shown. The dotted line denotes our overall 99% confidence upper limit of $a_{\rm x} \sin i \lesssim 0.26$ lt-s.

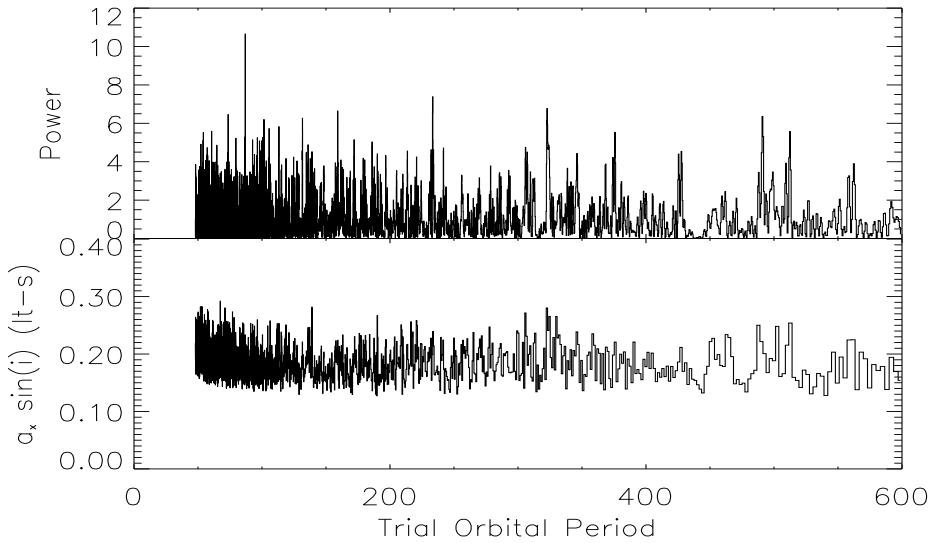

Fig. 6.— Lomb-Scargle periodogram and $a_{\rm x} \sin i$ upper limits for short ($\sim 2P_{\rm spin}$) intervals.

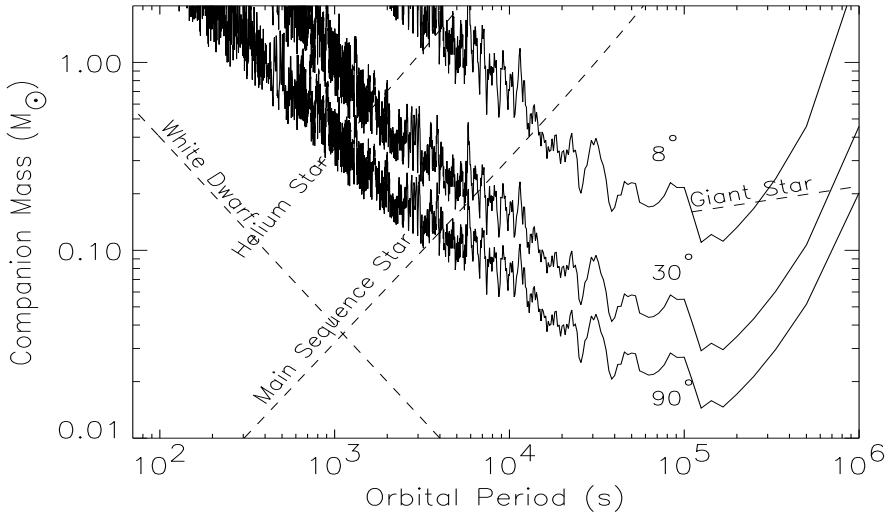

Fig. 7.— Companion mass limits calculated using the 99% confidence limits on $a_x \sin i$ from Figures 5 & 6, assuming a 1.4 $M_\odot$ neutron star and 8, 30, 90° inclination angles. Also shown are the period-mass relations for a normal main sequence star, helium burning star,and white dwarf and a period core mass relation for a giant star.